

# How to Differentiate between Near Field and Far Field: Revisiting the Rayleigh Distance

Shu Sun, Renwang Li, Xingchen Liu, Liuxun Xue, Chong Han, and Meixia Tao

**Abstract**—Future wireless communication systems are likely to adopt extremely large aperture arrays and millimeter-wave/sub-THz frequency bands to achieve higher throughput, lower latency, and higher energy efficiency. Conventional wireless systems predominantly operate in the far field (FF) of the radiation source of signals. As the array size increases and the carrier wavelength shrinks, however, the near field (NF) becomes non-negligible. Since the NF and FF differ in many aspects, it is essential to distinguish their corresponding regions. In this article, we first provide a comprehensive overview of the existing NF-FF boundaries, then introduce a novel NF-FF demarcation method based on effective degrees of freedom (EDoF) of the channel. Since EDoF is intimately related to spectral efficiency, the EDoF-based border is able to characterize key channel performance more accurately, as compared with the classic Rayleigh distance. Furthermore, we analyze the main features of the EDoF-based NF-FF boundary and provide insights into wireless system design.

## I. INTRODUCTION

THE deployment of the fifth-generation (5G) networks on a global scale has prompted both academia and industry to turn their attention to the development of the sixth-generation (6G) technologies. The major application scenarios of 5G include enhanced mobile broadband, massive machine type communications, and ultra-reliable and low latency communications, which are expected to support 20 Gbps peak data rate,  $10^6$  devices/km<sup>2</sup>, and 1 ms end-to-end latency, among others. However, 6G is poised to meet the demands of new and emerging applications, such as immersive cloud extended reality, holographic communications, sensory interconnection, and intelligent interaction. The burgeoning proliferation of wireless devices and their increasingly diverse applications has placed substantially higher demands on 6G in comparison to 5G. These demands encompass key performance metrics such as rate, reliability, latency, mobility, and energy consumption, with expectations typically being 10 to 100 times higher than those of 5G [1]. To achieve these ambitious vision and requirements for 6G, numerous key technologies have been proposed and are actively under development.

Notably, 6G is anticipated to leverage new spectrum resources, including the millimeter-wave (mmWave) and Tera-hertz (THz) bands. The shorter wavelengths in these bands, compared to the conventional microwave spectrum, allow for

Shu Sun, Renwang Li, Xingchen Liu, Liuxun Xue, and Meixia Tao are with the Department of Electronic Engineering and the Cooperative Medianet Innovation Center (CMIC), Shanghai Jiao Tong University, China. Chong Han is with Terahertz Wireless Communications (TWC) Laboratory, and with the Department of Electronic Engineering and CMIC, Shanghai Jiao Tong University, China.

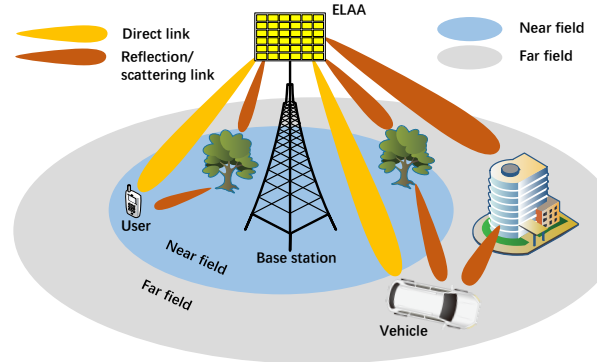


Fig. 1. Illustration of wireless communications in the near field and far field.

the integration of more antennas within a confined space. Consequently, the number of antennas continues to increase, evolving from the standard 64 antennas [2] to the scale of hundreds or even thousands [3]. This technological advancement has given rise to the concept of extremely large aperture arrays (ELAAs), which offer the potential for high beamforming gain, exceptional spatial resolution, and remarkable spectral efficiency [4].

The deployment of ELAA, in conjunction with tinier wavelengths of mmWave/THz bands, accentuates the NF (NF) effect. Generally, the electromagnetic (EM) field can be categorized into three regions: the reactive NF, the radiative NF, and the far field (FF). Since EM waves in the reactive NF are usually localized around the source and do not propagate, the radiative NF is more relevant to wireless communications, hence this article focuses on the radiative NF and refers to this as NF for simplicity. In the NF zone, which occurs when the communication distance is relatively small, the EM wavefronts are spherical. Here, factors such as the non-linear signal phase variations and differences in the traveling distance among different antennas in an ELAA need to be taken into account. The spherical wavefront model (SWM) considers the factors above, and is thus highly accurate, but involves high computational complexity. Conversely, when the communication distance extends to the FF regime, the SWM can be approximated by the planar wavefront model (PWM), since the angles at which the EM wave radiated from or received by each antenna in an array can be regarded as nearly identical. The PWM is a more simplified model, relying primarily on angle information and the number of antennas, making it highly convenient for channel modeling, performance analysis, and system design. As a result, the

PWM has been widely studied and implemented in 5G and earlier networks.

Due to the expansive array aperture of an ELAA, the NF region extends significantly, expanding from just a few meters for a conventional antenna array to hundreds of meters based on the classic Rayleigh distance [5] (to be introduced in more detail later on). Consequently, communication devices are more likely to be situated in the NF region, as depicted in Fig. 1, where a user and a vehicle are located in the NF and FF regions, respectively. Importantly, channel modeling in the NF and FF regions differs significantly. Specifically, the direct and reflection/scattering link in the NF should be characterized by the SWM, while the links in the FF can be reasonably approximated by the PWM. The reflectors/scatterers may be located in the NF and/or FF, which makes the propagation environment intricate. The Rayleigh distance, however, may not be the most proper NF-FF boundary in all wireless communication scenarios [6], and other criteria for demarcating the NF and FF are worth exploring.

## II. IMPACT OF NF-FF BOUNDARY ON IMPORTANT ASPECTS OF WIRELESS COMMUNICATIONS

In this section, we discuss the impact of the NF-FF boundary on various aspects of wireless communications systems, including antenna array characterization, propagation channel, and sensing as examples, which underscores the importance of investigating the NF-FF boundary.

### A. Impact on Antenna Array Characterization

Accurate evaluation of the NF and FF regimes of an antenna array is pivotal when conducting characterization and measurements of the array. Most antenna arrays are used in the FF (e.g., communication, radar, etc.). Hence, conducting array calibration in the FF ensures that the array radiates or receives as intended over long distances. NF array calibration is performed to ensure accurate array behavior when interacting with close-by objects or when the target application is within the NF zone. In the NF, interactions between the antenna elements can be much more intricate. These interactions, especially in large and closely spaced arrays, can lead to unpredictable effects like grating lobes or unwanted side lobes. Knowledge of the NF area helps in accurately characterizing these interactions. If characterization measurements are taken in the NF when they are assumed to be in the FF, significant errors can arise.

### B. Impact on Propagation Channel

The impact of the NF-FF boundary can also be observed in channel properties and characteristics such as path loss and spatial non-stationarity. Existing literature has unveiled that channel gain scales differently with distance in the NF and FF, thus it is critical to have accurate knowledge of the NF and FF regions so as to apply the corresponding power scaling laws. Furthermore, spatial non-stationarity, referring to the variability of the wireless channel characteristics over space, is another main difference in the channel. Spatial non-stationarity can occur in both the FF and NF. In the FF, spatial

non-stationarity is usually caused by large aperture of the antenna array at the BS, such that users at distinct locations may see different parts of the array and/or that the signals encounter different scatterers. While in the NF, besides the large array aperture, the non-linear phase shifts across array elements caused by the spherical wavefront also contribute to spatial non-stationarity, further complicating the situation. Therefore, it is imperative to have an accurate evaluation of the NF-FF boundary to ease the analysis.

### C. Impact on Sensing

Integrated sensing and communication (ISAC) is a paradigm where sensing and communication functionalities coexist. The NF-FF boundary remains central to shaping ISAC systems. In the NF, the spherical nature of the wavefronts facilitates the capture of fine details in sensing applications, given the wavefront's inherent ability to conform closely to intricate surfaces and interfaces. In the FF, the wavefronts tend to become planar over extended propagation distances. This transformation implies broader-scale sensing and a propensity for long-range, but potentially lower bandwidth, communication. Meanwhile, FF designs typically aims to achieve robust long-range propagation and broader sensing coverage.

## III. EXISTING RESEARCH RESULTS ON THE BOUNDARY BETWEEN NF AND FAR FIELD

As mentioned in the previous sections, reasonable demarcation of the NF and FF is momentous for wireless communication systems with ELAAs. In this section, we review existing research results on NF-FF boundaries, and classify them into two broad categories: multiple-input-single-output (MISO) or equivalently single-input-multiple-output (SIMO) system where only one communication link end is equipped with multiple antennas, and multiple-input-multiple-output (MIMO) system where both communication link ends possess multiple antennas.

### A. MISO/SIMO System

1) *Rayleigh Distance*: The classic border between the NF and FF of an antenna is called the *Rayleigh distance* or *Fraunhofer distance*,  $2D^2/\lambda$ , where  $D$  denotes the maximum aperture of the antenna and  $\lambda$  the carrier wavelength. The Rayleigh distance is defined from the perspective of the phase error: If the distance between a user and a base station (BS) is larger than  $2D^2/\lambda$ , then the maximum phase error across the antenna aperture between using the PWM and the SWM is no more than  $\pi/8$ . This definition is easily extendable to an antenna array, where  $D$  represents the array aperture. The Rayleigh distance reveals that the boundary between the NF and far field is proportional to the antenna/array aperture length squared, while inversely proportional to the carrier wavelength. It is commonly used to distinguish the near- and far-field regions since it can well capture the phase variations caused by the SWM and has a succinct mathematical expression. However, the Rayleigh distance has weak association with channel performance metrics, such as channel gain and channel capacity, which are important in practical wireless communications systems.

TABLE I  
EXISTING RESULTS ON NF-FF BOUNDARIES.

System	Boundary	Ref.	Antenna array configuration	Definition criterion	Distance formula	Distance characteristics
MISO or SIMO	Rayleigh distance	[5]	Single antenna to arbitrary array aperture	The maximum phase error does not exceed $\pi/8$ .	$\frac{2D^2}{\lambda}$	Classic distance boundary to distinguish the near- and far-field regions.
	Critical distance	[7]	Single antenna to ULA	The power ratio between the weakest and strongest array elements remains above a specified threshold.	$9D$	Focusing on the amplitude discrepancy.
	Uniform-power distance	[8]	Single antenna to UPA	The power ratio between the weakest and strongest array elements is no smaller than a threshold $\Gamma_{th}$ .	$\sqrt{\frac{\Gamma_{th}^{2/3}}{1-\Gamma_{th}^{2/3}} \frac{L_d}{2}}$	Additional consideration of the variation of the projected aperture across the antenna array.
	Effective Rayleigh distance	[9]	Single antenna to ULA	The normalized beamforming gain under the far-field assumption is no less than 95%.	$0.367 \cos^2(\theta) \frac{2D^2}{\lambda}$	Can be seen as a correction for the Rayleigh distance to ensure the beamforming gain when adopting the PWM.
	Björnson distance	[10]	Single antenna to UPA	The normalized antenna array gain is close to 1.	$2L\sqrt{N}$	Achieving almost the maximum antenna array gain.
	Equi-power line	[11]	Single antenna to ULA	The normalized received power is close to 1.	$2.86D$	Considering both the amplitude and phase discrepancy. The PWM always overestimates the received power when $ \theta  \leq \pi/6$ .
	Equi-power surface	[11]	Single antenna to UCPA	The normalized received power is close to 1.	$3.96D$	Considering both the amplitude and phase discrepancy. The PWM always overestimates the received power when $\cos^2(\phi) \cos^2(\varphi) \geq 1/2$ .
MIMO	Rayleigh distance	[5]	Arbitrary array apertures	The maximum phase error does not exceed $\pi/8$ .	$\frac{2(D_T+D_R)^2}{\lambda}$	Classic distance boundary to distinguish the near- and far-field regions.
	Threshold distance in [12]	[12]	ULA to ULA	The capacity of the SWM surpasses that of the PWM by at least a factor of 1.5.	$4L_T L_R \cos(\theta_T) \cos(\theta_R)$	Can be regarded as the 0.225 dB-down beamwidth distance of the array.
	Threshold distance in [13]	[13]	ULA to ULA	The ratio of the largest eigenvalues, as given by SWM and PWM, reaches a pre-defined threshold.	$\frac{\tau_g d_T d_R \cos(\theta_T) \cos(\theta_R)}{\lambda}$	Only considering the largest eigenvalue. Accurate when the antenna number is small.
	Effective multiplexing distance	[14]	ULA to ULA	The channel can efficiently accommodate $m$ independent spatial streams simultaneously at a specific SNR.	$\frac{D_T D_R}{\lambda S_{asy,m}^*(\gamma)}$	Efficient for two independent spatial streams.

Note:  $D$  denotes the array aperture.  $\lambda$  denotes the carrier wavelength.  $\Gamma_{th}$  is a threshold smaller than one.  $L_d$  denotes the diagonal dimension of the UPA.  $\theta$  is the incident angle.  $L$  represents the diagonal length of each antenna element.  $N$  represents the antenna number.  $D_T$  and  $D_R$  denote the array aperture at the Tx and Rx, respectively.  $L_T$  and  $L_R$  represent the array size in units of wavelength at the Tx and Rx, respectively.  $\theta_T$  and  $\theta_R$  denote the rotated angle at the Tx and Rx, respectively.  $\tau_g$  and  $S_{asy,m}^*(\gamma)$  are auxiliary variables.

2) *Critical Distance*: The Rayleigh distance primarily pertains to the maximum acceptable phase difference among array elements. However, when employing the optimal maximum ratio combining (MRC), the signal phases can be perfectly aligned, eliminating their impact on the received power. In this context, the received power relies solely on the amplitude response of the channel. Consequently, the authors in [7] propound a critical distance  $r_{Critical}$ . This critical distance ensures that the power ratio between the weakest and strongest array elements remains above a specified threshold, effectively leading to an approximation of  $r_{Critical} \approx 9D$ , with  $D$  repre-

senting the antenna aperture. Denote the Rayleigh distance as  $r_{Ray}$ , the communication distance  $r$  can be divided into three intervals: 1) For  $r \geq r_{Ray}$ , both the amplitude and phase differences across the antenna array are small, allowing for a safe approximation using the PWM; 2) For  $r_{Critical} \leq r < r_{Ray}$ , while amplitude differences are relatively small and thus negligible, significant phase differences persist across the antenna array and cannot be disregarded; 3) For  $r < r_{Critical}$ , both amplitude and phase variations are substantial. Consequently, the channel should be modeled utilizing the SWM.

3) *Uniform-Power Distance*: The critical distance in [7] is extended to the uniform-power distance (UPD) in [8] by additional considerations of UPA structure and the variation of the projected aperture across the antenna array. The UPD maintains the same definition as in [7], [8], defining a distance beyond which the power ration between the weakest and strongest array elements is no smaller than a certain threshold  $\Gamma_{th}$ . When the Rx is positioned at the center of and aligned perpendicularly to the UPA, the UPD can be explicitly expressed as  $\sqrt{\frac{\Gamma_{th}^{-2/3} L_d}{1-\Gamma_{th}^{-2/3}}}$ , where  $L_d$  denotes the diagonal dimension of the UPA. For other incident angles and positions, the UPD can be obtained numerically.

4) *Effective Rayleigh Distance*: The authors in [7] and [8] adopt the optimal MRC to eliminate the influence of the signal phases. However, due to the inherent challenges in achieving perfect channel estimation, and the MRC may not completely cancel out the phases. Therefore, from a beamforming perspective, the authors in [9] propose an effective Rayleigh distance  $R_{eff}$ , beyond which the normalized beamforming gain under the far field assumption is no less than 95%. The effective Rayleigh distance is given by  $R_{eff} = 0.367 \cos^2(\theta) \frac{2D^2}{\lambda}$ , where  $\theta$  is the incident angle,  $D$  is the antenna aperture, and  $\lambda$  is the carrier wavelength. The effective Rayleigh distance can be seen as a correction for the Rayleigh distance to ensure the beamforming gain when adopting the PWM.

5) *Björnson Distance*: The authors in [10] consider a UPA structure consisting of  $N$  identical antennas, each with an area denoted as  $A$ . From a strict electromagnetic perspective, they introduce a normalized antenna array gain, representing the received power relative to the power obtained in the far field under the PWM. Under this modeling, the Rayleigh distance can be re-expressed as  $d_{Ray} = 2NL^2/\lambda$ , where  $L = \sqrt{2A}$  denotes the diagonal length of each antenna element. Then, they propose the Björnson distance as  $d_b = 2L\sqrt{N}$ . Notably, the Björnson distance exhibits growth proportional to the square root of  $N$ , in contrast to the linear growth with  $N$  seen in the Rayleigh distance. At least 95% of the maximum gain can be achieved when the communication distance is no less than the Björnson distance.

6) *Equi-Power Line*: Considering a ULA structure with only a line-of-sight (LoS) path, the received power under the MRC from a point source is solely determined by the amplitude response and is independent of the signal phase. The authors in [11] define a ratio of the received power obtained with the SWM to that obtained with the PWM. When the communication distance goes to infinity, the ratio tends towards one. They propose an equi-power line, which represents this ratio reaches a pre-defined threshold. The closed-form analytical expression for this ratio leads to an equi-power line located at approximately  $2.86D$  with  $D$  representing the array aperture, when the source aligns perpendicularly with the middle of the ULA. For other source angles, numerical methods are employed to determine the equi-power line. Interestingly, the study reveals that within the incident angle range of  $[-\pi/6, \pi/6]$ , the received power under PWM consistently serves as an upper bound for that under SWM. Beyond this range, as the distance increases, the power corresponding to

PWM initially functions as an upper bound but subsequently transforms into a lower bound for the power under SWM.

7) *Equi-Power Surface*: Considering a uniform circular planar array (UCPA) structure with only an LoS path, the received power under the MRC from a point source only relies on the amplitude response. The authors in [11] define a normalized received power, which signifies the relative received power obtained by the SWM compared to the PWM. Subsequently, they propound an equi-power surface at which the normalized received power attains a predefined threshold. Utilizing a derived closed-form expression, the equi-power line is situated at approximately  $3.96D$  with  $D$  representing the length of the side of the UCPA, when the source is perpendicular to the center of the UCPA. When the source is located in other angles, the equi-power line can be obtained numerically.

## B. MIMO System

For the MIMO system, a widely recognized NF-FF boundary is the extended version of the Rayleigh distance defined as  $2(D_T + D_R)^2/\lambda$ , where  $D_T$  and  $D_R$  denote the maximum array aperture at the transmitter (Tx) and receiver (Rx), respectively.

1) *Threshold Distance in [12]*: The authors in [12] propose a threshold distance below which the capacity of the SWM surpasses that of the PWM by at least a factor of 1.5, given a specific array size. In practical terms, this threshold distance marks a point where the capacity underestimation error when using the PWM is 50%. By using the empirical fitting techniques, they derive the threshold distance as  $4L_T L_R \cos(\theta_T) \cos(\theta_R)$ , where  $L_T$  ( $L_R$ ) is the array size at the Tx (Rx) in units of wavelength, and  $\theta_T$  ( $\theta_R$ ) is the rotated angle at the Tx (Rx). Note that this threshold distance is in units of wavelength. This threshold distance can also be regarded as the 0.225 dB-down beamwidth distance of the array. When considering the half-power beamwidth (3 dB) of the array, the threshold distance can be calculated as  $1.13L_T L_R \cos(\theta_T) \cos(\theta_R)$ .

2) *Threshold Distance in [13]*: Building upon an approximation of the largest eigenvalue of LoS MIMO channels employing uniform linear arrays (ULA) structure, the authors in [13] obtain a threshold distance at which the ratio of the largest eigenvalues, as given by SWM and PWM, reaches a predefined threshold. This threshold distance is given by  $\tau_g d_T d_R \cos(\theta_T) \cos(\theta_R)/\lambda$ , where  $d_T$  ( $d_R$ ) is the antenna spacing at the Tx (Rx),  $\theta_T$  ( $\theta_R$ ) is the rotated angle at the Tx (Rx), and  $\tau_g$  is an auxiliary variable which is dependent on the antenna number of the Tx and Rx. The exact value of  $\tau_g$  can be found in [13]. This approach is relatively accurate when the antenna number is small. However, when the antenna number is large, the exact largest eigenvalue cannot be obtained. Moreover, this approach solely considers the largest eigenvalue, which imposes limitations on the accuracy of the threshold distance.

3) *Effective Multiplexing Distance*: Considering spatial multiplexing, the authors in [14] propose an effective multiplexing distance  $D_{max}^{(m)}$ . This distance represents the farthest range at which the channel can efficiently accommodate  $m$

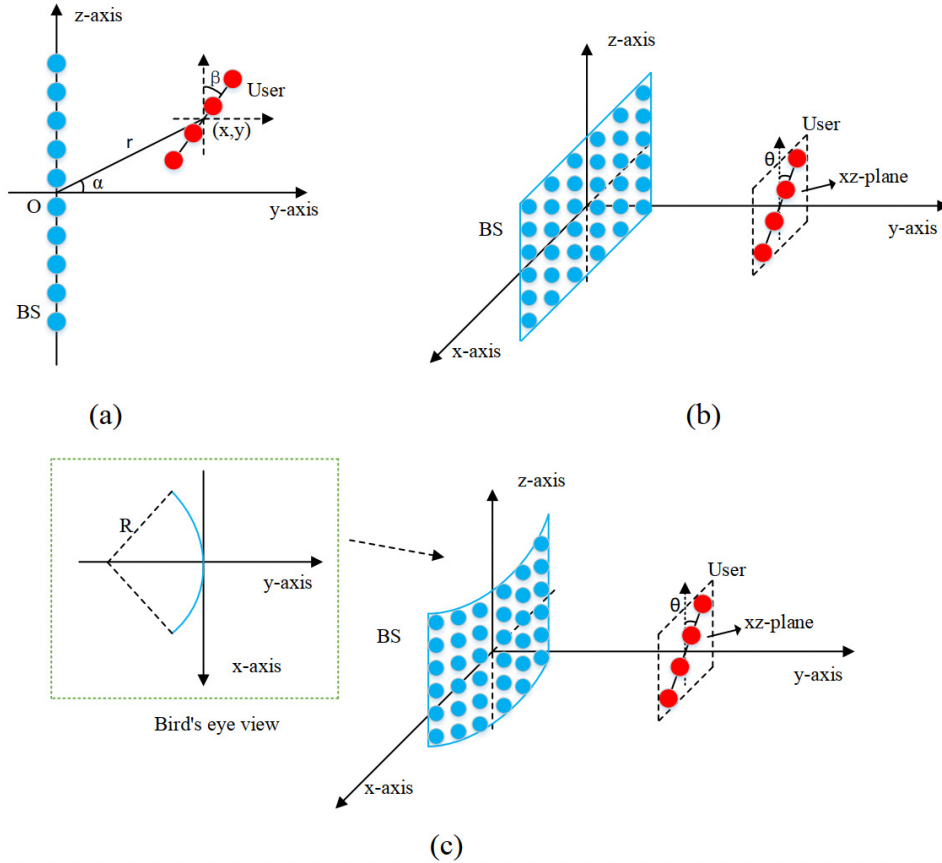


Fig. 2. Antenna array configurations considered in this article. (a) Both the BS and user are equipped with a ULA, where  $\alpha$  denotes the angle between the center of the BS ULA and the center of the user ULA, and  $\beta$  is the angle of the user ULA with respect to the positive Z-direction within the YZ-plane. (b) The BS and user are equipped with a URA and a ULA, respectively, where  $\theta$  represents the angle of the user ULA with respect to the positive Z-direction and parallel with the XZ-plane. (c) The BS and user are equipped with an arched “URA” and a ULA, respectively, where the edge of the URA along the X-direction is arched according to a certain curvature radius  $R$ , while  $\theta$  represents the angle of the user ULA with respect to the positive Z-direction and parallel to the XZ-plane. It is further postulated that the horizontal edge of the URA form part of a semicircular arc with a curvature radius of  $R$ , hence the semicircular cylindrical surface can be regarded as a special case of the arched URA architecture with the horizontal edge being a complete semicircular arc.

independent spatial streams simultaneously at a specific signal-to-noise ratio (SNR). The effective multiplexing distance can be approximated by  $D_{\max}^{(m)} \approx D_T D_R / (\lambda \tilde{S}_{\text{asy},m}^*(\gamma))$ , where  $D_T$  ( $D_R$ ) is the array aperture at the Tx (Rx),  $\lambda$  is the carrier wavelength,  $\gamma$  is the SNR requirement, and  $\tilde{S}_{\text{asy},m}^*(\gamma)$  is an auxiliary variable that accounts for the threshold at which the MIMO system can support  $m$  independent spatial streams under the given SNR  $\gamma$ . The specific values of  $\tilde{S}_{\text{asy},m}^*(\gamma)$  can be determined through numerical simulations. Denoting the Rayleigh distance as  $r_{\text{Ray}}$ , the communication distance  $D$  can be categorized into three intervals: 1) For  $D \in (0, r_{\text{Ray}}]$ , the MIMO system can consistently achieve the full multiplexing gain by adjusting the orientations of the antennas; 2) For  $D \in (r_{\text{Ray}}, D_{\max}^{(m)})$ , the MIMO system can effectively support  $m$  streams at the specified SNR  $\gamma$ ; 3) For  $D \in (D_{\max}^{(m)}, \infty)$ , the channel exhibits only one dominant eigenvalue, thus supporting a single stream.

#### IV. PROPOSED DEMARCATION BASED ON EFFECTIVE DEGREES OF FREEDOM

In this section, we first introduce a new NF-FF demarcation criterion focusing on the effective degrees of freedom (EDoF)

of the channel, then investigate the characteristics of the EDoF-based boundary in typical application scenarios and its implications for system performance.

##### A. Demarcation Criterion

For a MIMO system, channel capacity is a commonly utilized criterion to evaluate the system performance, which represents the information-transmission ability of a communication system. Channel capacity is closely related to the EDoF of the channel, where the EDoF represents the equivalent number of single-input-single-output sub-channels<sup>1</sup>. An information-theory-originated definition of the EDoF is  $\left(\frac{\text{tr}(\mathbf{R})}{\|\mathbf{R}\|_F}\right)^2$  [15], where  $\mathbf{R}$  denotes the spatial correlation matrix of the MIMO channel matrix, while  $\text{tr}(\cdot)$  and  $\|\cdot\|_F$  denote the trace and Frobenius norm of a matrix, respectively. In order to characterize the channel performance (e.g., channel capacity) more accurately, we introduce a novel NF-FF demarcation approach based upon the EDoF. Specifically, the boundary  $r_{\text{Th}}$  between the NF and FF is defined such that the EDoF

<sup>1</sup>For simplicity, this article considers single polarization and focuses on the spatial aspect of the degrees of freedom of the channel.

TABLE II  
EDoF-BASED NF-FF BOUNDARY  $r_{\text{Th}}$  FOR DIFFERENT ANTENNA ARRAY CONFIGURATIONS

Antenna Array Configurations of Tx and Rx	ULA, ULA	URA, ULA	Arched URA, ULA
General Case	$r_{\text{Th}} \approx \frac{\pi L_{\text{T}} L_{\text{R}}}{(N_{\text{T}}-1)(N_{\text{R}}-1)\lambda b},$ <p>where <math>b</math> satisfies</p> $\sum_{n=1}^{N_{\text{R}}-1} (N_{\text{R}} - n) \left[ \frac{\sin(nN_{\text{T}}b)}{\sin(nb)} \right]^2 = \frac{1}{2} \left( \frac{N_{\text{T}}^2 N_{\text{R}}^2}{\eta} - N_{\text{T}}^2 N_{\text{R}} \right)$	$r_{\text{Th}} \approx \frac{\pi L_{\text{R}} L_{\text{T}_x} \sin(\theta)}{(N_{\text{T}_x}-1)(N_{\text{R}}-1)\lambda b} = \frac{\pi L_{\text{R}} L_{\text{T}_z} \cos(\theta)}{(N_{\text{T}_z}-1)(N_{\text{R}}-1)\lambda g}$ <p>where <math>b</math> and <math>g</math> satisfy</p> $\sum_{n=1}^{N_{\text{R}}-1} (N_{\text{R}} - n) \left[ \frac{\sin(nN_{\text{T}_x}b)\sin(nN_{\text{T}_z}g)}{\sin(nb)\sin/ng} \right]^2 = \frac{1}{2} \left( \frac{N_{\text{T}}^2 N_{\text{R}}^2}{\eta} - N_{\text{T}}^2 N_{\text{R}} \right)$	$r_{\text{Th}}$ approaching that for the {URA, ULA} configuration when $R \geq L_{\text{arch}}$
Special Case 1: $N_{\text{R}} = 2$ , ULA: $N_{\text{T}} = 2$ , URA: $N_{\text{T}_x} = N_{\text{T}_z} = 2$	$r_{\text{Th}} \approx \frac{\pi L_{\text{T}} L_{\text{R}}}{\lambda \times \arccos\left(\sqrt{\frac{2}{\eta}-1}\right)}$	$r_{\text{Th}} \approx \frac{\pi L_{\text{T}_x} L_{\text{R}} \sin(\theta)}{\lambda b}, \text{ where } b \text{ satisfies } \frac{\sin(2b)\sin(2bg)}{\sin(b)\sin(bg)} = 4\sqrt{\frac{2}{\eta}-1}, g = \frac{L_{\text{T}_z} \cos(\theta)}{L_{\text{T}_x} \sin(\theta)}$	
Special Case 2: $N_{\text{T}} \rightarrow \infty, N_{\text{R}} = 2$	$r_{\text{Th}} \approx \frac{\pi L_{\text{T}} L_{\text{R}}}{\lambda b},$ <p>where <math>b</math> satisfies <math>\frac{\sin(b)}{b} = \sqrt{\frac{2}{\eta}-1}</math></p>	$r_{\text{Th}} \approx \frac{\pi L_{\text{T}_x} L_{\text{R}} \sin(\theta)}{\lambda b}, \text{ where } b \text{ satisfies } \frac{\sin(b)\sin(bg)}{b^2 g} = \sqrt{\frac{2}{\eta}-1}, g = \frac{L_{\text{T}_z} \cos(\theta)}{L_{\text{T}_x} \sin(\theta)}$	
Special Case 3: $N_{\text{T}} \rightarrow \infty, N_{\text{R}} \rightarrow \infty$	$r_{\text{Th}} \approx \frac{\pi L_{\text{T}} L_{\text{R}}}{\lambda b},$ <p>where <math>b</math> satisfies</p> $\frac{2b\text{Si}(2b)+\text{Ci}(2b)-2\sin^2(b)-\ln(2b)-0.5772}{b^2} = \frac{1}{\eta}$	$r_{\text{Th}} \text{ approximately proportional to } \frac{\pi L_{\text{R}} \sqrt{L_{\text{T}_x}^2 \sin^2(\theta) + L_{\text{T}_z}^2 \cos^2(\theta)}}{\lambda}$	

Note: *Arched URA* denotes the ‘‘URA’’ with one of its edges arched according to a certain curvature radius.  $\eta$ ,  $L_{\text{T}}$ ,  $L_{\text{R}}$ ,  $N_{\text{T}}$ , and  $N_{\text{R}}$  respectively represent the target EDoF of the MIMO channel, aperture of the Tx antenna array, aperture of the Rx antenna array, number of elements of the Tx array, and number of elements of the Rx array,  $L_{\text{T}_x}$ ,  $L_{\text{T}_z}$ ,  $N_{\text{T}_x}$ , and  $N_{\text{T}_z}$  respectively denote the horizontal side length of the URA, vertical side length of the URA, number of elements along the horizontal direction of the URA, and number of elements along the vertical direction of the URA,  $\theta$  is the rotation angle depicted in Fig. 2, while  $R$  and  $L_{\text{arch}}$  stand for the curvature radius and the length of the arched edge of the URA, respectively. These results are obtained under the paraxial approximation in optics, i.e., the distance between the Tx and Rx arrays is significantly larger than their apertures.

of the MIMO system equals a pre-defined threshold  $\eta$  at  $r_{\text{Th}}$  under the SWM. Since the EDoF is 1 under the PWM when only an LoS path exists between the Tx and Rx, the threshold value of EDoF  $\eta$  can be set to a value slightly larger than 1. This EDoF demarcation criterion can capture the differential spatial characteristics of the MIMO system between the SWM and PWM, and is more explicitly related to key performance indicators, such as the capacity and multiplexing capability, of the channel.

### B. Case Studies

In the sequel, we will unveil the main behaviors of the proposed EDoF-based NF-FF boundary and how it differs from the classic Rayleigh distance through some examples. We consider point-to-point MIMO systems, as illustrated in Fig. 2, where the user is equipped with a ULA, and the antenna array at the BS can be a ULA or a URA. It is noteworthy that besides the conventional ULA and URA, we also take into account an arched ‘‘URA’’ architecture (shown in Fig. 2(c)),

in which one of the edges of the URA is bent according to a certain curvature radius. This is motivated by the advanced conformal antenna array whose surface can be flexibly bent based on the shape of the object it situates on. Detailed settings are described in the figure caption.

Based upon the aforementioned EDoF formula  $\left(\frac{\text{tr}(\mathbf{R})}{\|\mathbf{R}\|_{\text{F}}}\right)^2$ , we conduct mathematical derivations (not shown in this article) for the three types of MIMO systems in Fig. 2 to obtain accurate or approximate expressions of the NF-FF boundary  $r_{\text{Th}}$ , and provide the results in Table II<sup>2</sup>. Note that these results are obtained under the paraxial approximation in optics, i.e., the distance between the Tx and Rx arrays is significantly larger than their apertures, which is practical in many real-world communication systems. For the ULA-to-ULA scenario, it is evident from the expression of  $r_{\text{Th}}$  that unlike the

<sup>2</sup>The purpose of displaying those mathematical equations in Table II is not to delve into details of the expressions, but to provide explicit forms of the EDoF-based boundary so as to make it more convenient to exposit its key influencing factors.

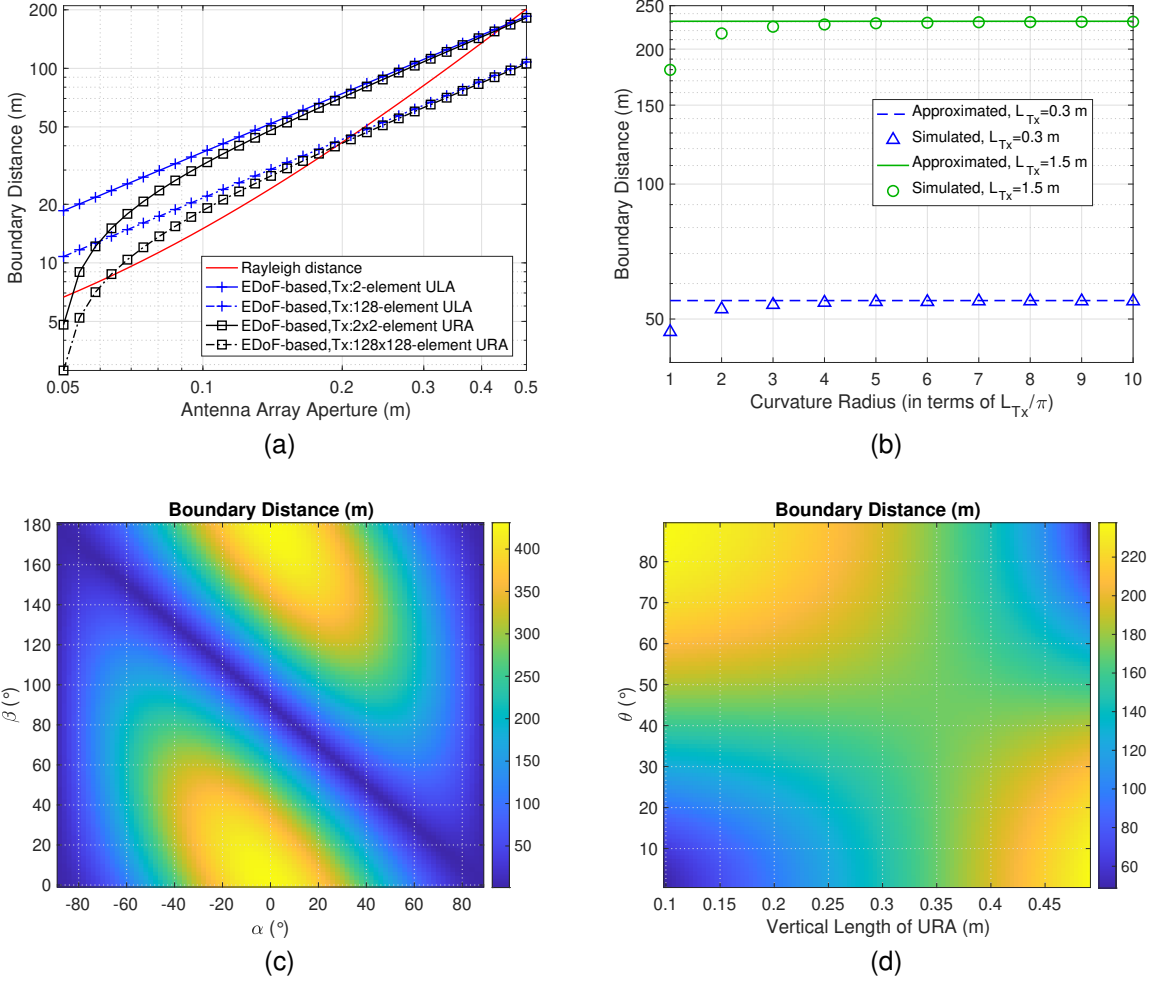


Fig. 3. Characterization of the EDoF-based NF-FF boundary under various circumstances. (a) Comparison of different NF-FF boundaries, where the Rx is equipped with a two-element ULA with a length of 0.05 m, the horizontal side length of the Tx URA is fixed to 0.049 m, the orientation angle  $\theta$  in Fig. 2(b) is set to  $10^\circ$ , and the X-axis values denote the maximum aperture of the Tx ULA or URA. (b) EDoF-based boundary for the arched URA in Fig. 2(c), in which the approximated values are calculated according to the URA results in Table II, and the simulated values are obtained via numerical simulation using the actual arched array architecture. The vertical length of the arched URA is 0.2 m, the length of the ULA is 0.05 m, and the orientation angle  $\theta$  of the ULA is  $45^\circ$ . (c) Variation of the EDoF-based boundary with the position and orientation angles  $\alpha$  and  $\beta$  depicted in Fig. 2(a). The lengths of the Tx and Rx ULAs are 1 m and 0.1 m, respectively, and the numbers of elements of the Tx and Rx ULAs are 128 and 2, respectively. (d) Variation of the EDoF-based boundary with the orientation angle  $\theta$  and the vertical length of the URA depicted in Fig. 2(b). The aperture of the URA is 0.5 m, and the numbers of elements along the horizontal and vertical directions of the URA are both eight. The ULA has two elements and its length is 0.1 m.

Rayleigh distance which relies on the square of the sum of the Tx array aperture  $L_T$  and the Rx array aperture  $L_R$ , the EDoF-based boundary  $r_{Th}$  is related to the product of  $L_T$  and  $L_R$ , as well as the numbers of array elements at the Tx and Rx  $N_T$  and  $N_R$ , respectively. More specifically,  $r_{Th}$  is proportional to  $\pi L_T L_R$  and inversely proportional to  $(N_T - 1)(N_R - 1)\lambda$ , indicating that  $r_{Th}$  will alter if the number of array elements at either the Tx or Rx changes, even if both array lengths remain the same. Furthermore, fewer array elements correspond to a larger boundary distance, thus the boundary for an array with two elements serves as an upper bound while that for an infinite number of array elements acts as a lower bound. For the URA-to-ULA scenario, assuming the ULA is equipped at the Rx,  $r_{Th}$  is still proportional to  $\pi L_R$  and inversely proportional to  $(N_R - 1)\lambda$ , whereas its relation with the size and number of elements of the URA

is more complicated. When fixing the horizontal (vertical) side length  $L_{Tx}$  of the URA,  $r_{Th}$  is proportional to the vertical (horizontal) side length  $L_{Tz}$ , and similar rules apply to the number of elements  $N_{Tx}$  and  $N_{Tz}$  along the horizontal and vertical directions; when both side lengths of the URA vary,  $r_{Th}$  depends on the product of the sinusoidal functions containing  $\frac{L_{Tx}}{N_{Tx}-1}$  and  $\frac{L_{Tz}}{N_{Tz}-1}$ . In addition, it is worth noting that when  $\theta = 0^\circ$  ( $90^\circ$ ),  $r_{Th}$  becomes independent of the side length and number of elements along the horizontal (vertical) direction of the URA. In other words,  $r_{Th}$  is proportional to the effective URA aperture  $\sqrt{L_{Tx}^2 \sin^2(\theta) + L_{Tz}^2 \cos^2(\theta)}$  projected onto the direction that the ULA lies in. For the arched-URA-to-ULA case, the mathematical derivation shows that  $r_{Th}$  is approximately identical to that for the URA-to-ULA setting if the curvature radius  $R$  is obviously larger than the arc length.

Next, we provide quantitative analysis on the EDoF-based

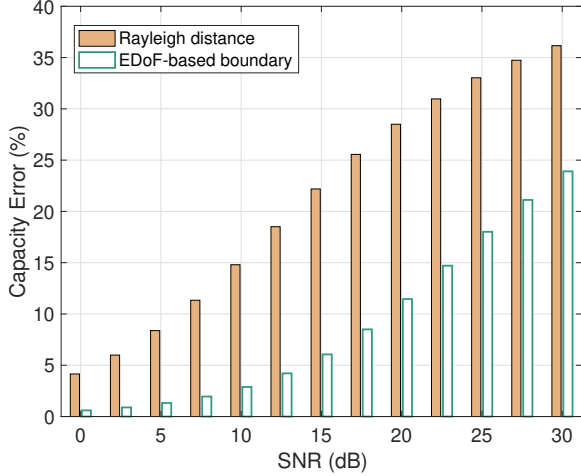


Fig. 4. Estimation error of the channel capacity at the Rayleigh distance and the EDoF-based boundary. Both the Tx and Rx are equipped with a two-element ULA, whose lengths are both 0.05 m, and the Rayleigh distance and the EDoF-based boundary herein are 6.67 m and 18.54 m, respectively.

NF-FF boundary values to gain more intuitive insights. In all the simulations, the EDoF threshold  $\eta$  is set to 1.01, and the carrier frequency is 100 GHz. Fig. 3 demonstrates EDoF-based NF-FF boundary values under a variety of circumstances, where the simulation settings are detailed in the figure caption. Several relevant observations can be drawn from Fig. 3: First, the Rayleigh distance can be smaller or larger than the EDoF-based boundary, as delineated in Fig. 3(a), implying that it may underestimate or overestimate the NF region from the viewpoint of supportable spatial streams. Second, since the length of the Rx ULA is fixed, the EDoF-based boundary grows linearly with the Tx array aperture for the ULA-to-ULA scenario, whereas the increasing trend is non-linear with respect to the URA aperture for the URA-to-ULA case, which is consistent with the results in Table II. Third, Fig. 3(b) reveals that the analytical expression of the EDoF-based boundary for the arched URA is sufficiently accurate when the curvature radius  $R$  is no smaller than  $3L_{Tx}/\pi$ , or roughly  $L_{Tx}$ , i.e., the curvature radius is no smaller than the arc length. Moreover, it is seen from Fig. 3(c) that the boundary distance reaches its maximum when the two ULAs are normally facing each other with the line of centers perpendicular to them, and arrives at its minimum when the line of centers of the two ULAs is aligned with one of the ULAs. Additionally, the boundary distance increases with the orientation angle  $\theta$  in the URA-to-ULA scenario when the vertical length of the URA is small, and behaves oppositely for a large vertical length, due to the fact that the boundary is proportional to the effective URA aperture  $\sqrt{L_{Tx}^2 \sin^2(\theta) + L_{Tx}^2 \cos^2(\theta)}$  as analyzed above.

### C. Implications for System Design

1) *Channel Capacity*: The NF-FF boundary has a crucial impact on channel capacity, since it determines the applicable regions of different electromagnetic wavefronts which in turn dictate the channel model. It has been shown in

Fig. 3(a) that the classic Rayleigh distance may underestimate or overestimate the NF zone depending on the antenna array configurations. Overestimation of the NF range can give rise to unnecessary computational complexity using the SWM, while underestimation may cause prediction error of the channel capacity. For instance, Fig. 4 depicts the estimation error of the channel capacity for a ULA-to-ULA wireless communication scenario, where the estimation error is computed by comparing the channel capacity using the PWM with that using the SWM at the corresponding boundary distance. As evident from Fig. 4, the Rayleigh distance leads to large capacity errors for a wide range of SNR values, and the capacity error can reach over 35% which is non-negligible and will seriously affect the system deployment strategies.

2) *Multiple Access*: The FF channel is dependent on the angle, making it unable to distinguish users located in the same direction. In contrast, the NF channel can discern both the angle and distance, allowing it to focus on a specific location even when multiple users share the same direction. To gain more insights into how the NF-FF boundary influences multiple access, we can regard the two-element ULA in the aforementioned simulations as two users each with a single antenna. In this sense, the boundary distance in Fig. 3(c) and Fig. 3(d) implies the distance at which the spatial channels between the two users are approximately fully correlated. As illustrated by Fig. 3(c) and interpreted in the previous subsection, the boundary distance reaches its minimum when the two users situate in the same direction from the viewpoint of the center of the BS antenna array, which is as expected since they share the direction. Nevertheless, the boundary distance is non-zero, indicating that their spatial channels are still distinguishable up to a certain distance from the BS. On the other hand, the two users are most easily discernible when their relative directions are the farthest apart (corresponding to the largest boundary distance in Fig. 3(c)) given a fixed distance between them. Furthermore, it can be inferred from Fig. 3(d) that the spatial channels between two users are less correlated when the line connecting them is parallel to the longer side of a URA. Consequently, if solely aiming to serve more users in the NF, it is beneficial to place the URA at the BS such that its longer side is parallel to the direction with most users. In practice, of course, other factors need also to be taken into account in system design. It is apparent from the foregoing examples that knowledge of how the NF-FF boundary varies with the azimuth and elevation angles is helpful in designing adaptive algorithms for channel estimation, beamforming/beam-focusing, and beam management, so as to sense and serve different users more efficiently based on their locations and relative orientations.

## V. CONCLUSION

In this article, we discussed the importance of identifying the NF regime for ELAAs, summarized existing NF-FF boundaries, and propounded a novel NF-FF demarcation scheme based on the EDoF of the MIMO channel. We investigated the key influencing factors and behaviors of the EDoF-based boundary for various antenna array configurations, including conformal antenna arrays, and analyzed the implications for

system design. The proposed NF-FF boundary is able to more accurately characterize system performance indicators such as channel capacity, as compared to the classic Rayleigh distance, and can provide more insights into wireless system deployment.

#### REFERENCES

- [1] Z. Wang, Y. Du, K. Wei, K. Han, X. Xu, G. Wei, W. Tong, P. Zhu, J. Ma, J. Wang *et al.*, “Vision, application scenarios, and key technology trends for 6G mobile communications,” *Science China Information Sciences*, vol. 65, no. 5, pp. 1–27, Mar. 2022.
- [2] J. Zhang, E. Björnson, M. Matthaiou, D. W. K. Ng, H. Yang, and D. J. Love, “Prospective multiple antenna technologies for beyond 5G,” *IEEE Journal on Selected Areas in Communications*, vol. 38, no. 8, pp. 1637–1660, Aug. 2020.
- [3] Y. Zhu, H. Guo, and V. K. N. Lau, “Bayesian channel estimation in multi-user massive MIMO with extremely large antenna array,” *IEEE Transactions on Signal Processing*, vol. 69, pp. 5463–5478, 2021.
- [4] E. D. Carvalho, A. Ali, A. Amiri, M. Angelichinoski, and R. W. Heath, “Non-stationarities in extra-large-scale massive MIMO,” *IEEE Wireless Communications*, vol. 27, no. 4, pp. 74–80, Aug. 2020.
- [5] K. T. Selvan and R. Janaswamy, “Fraunhofer and fresnel distances: Unified derivation for aperture antennas,” *IEEE Antennas and Propagation Magazine*, vol. 59, no. 4, pp. 12–15, Aug. 2017.
- [6] C. Han, Y. Chen, L. Yan, Z. Chen, and L. Dai, “Cross far- and near-field wireless communications in terahertz ultra-large antenna array systems,” *IEEE Wireless Communications*, to appear, 2023. [Online]. Available: <https://arxiv.org/pdf/2301.03035>.
- [7] H. Lu and Y. Zeng, “How does performance scale with antenna number for extremely large-scale MIMO?” in *ICC 2021-IEEE International Conference on Communications*. IEEE, Jun. 2021, pp. 1–6.
- [8] —, “Communicating with extremely large-scale array/surface: Unified modeling and performance analysis,” *IEEE Transactions on Wireless Communications*, vol. 21, no. 6, pp. 4039–4053, 2022.
- [9] M. Cui and L. Dai, “Near-field wideband beamforming for extremely large antenna array,” *arXiv preprint arXiv:2109.10054*, 2023. [Online]. Available: <https://arxiv.org/pdf/2109.10054>
- [10] E. Björnson, Ö. T. Demir, and L. Sanguinetti, “A primer on near-field beamforming for arrays and reconfigurable intelligent surfaces,” in *2021 55th Asilomar Conference on Signals, Systems, and Computers*, 2021, pp. 105–112.
- [11] R. Li, S. Sun, and M. Tao, “Applicable regions of spherical and plane wave models for extremely large-scale array communications,” 2023. [Online]. Available: <https://arxiv.org/abs/2301.06036>
- [12] J.-S. Jiang and M. Ingram, “Spherical-wave model for short-range MIMO,” *IEEE Transactions on Communications*, vol. 53, no. 9, pp. 1534–1541, Sep. 2005.
- [13] F. Bohagen, P. Orten, and G. E. Oien, “On spherical vs. plane wave modeling of line-of-sight MIMO channels,” *IEEE Transactions on Communications*, vol. 57, no. 3, pp. 841–849, Mar. 2009.
- [14] P. Wang, Y. Li, X. Yuan, L. Song, and B. Vucetic, “Tens of gigabits wireless communications over E-Band LoS MIMO channels with uniform linear antenna arrays,” *IEEE Transactions on Wireless Communications*, vol. 13, no. 7, pp. 3791–3805, Jul. 2014.
- [15] S. Verdu, “Spectral efficiency in the wideband regime,” *IEEE Transactions on Information Theory*, vol. 48, no. 6, pp. 1319–1343, 2002.